



Simultaneous negative reflection and refraction and reverse-incident right-angle collimation of sound in a solid-fluid phononic crystal

Yuqi Jin, 1,a) Ezekiel Walker, Tae-Youl Choi, Arup Neogi, 1,b) and Arkadii Krokhin, Dollar Die Neogi, 1,b)

ABSTRACT:

The square lattice phononic crystal (PnC) has been used extensively to demonstrate metamaterial effects. Here, positive and negative refraction and reflection are observed simultaneously due to the presence of Umklapp scattering of sound at the surface of PnC and square-like equifrequency contours (EFCs). It is found that a shift in the EFC of the third transmission band away from the center of the Brillouin zone results in an effectively inverted EFC. The overlap of the EFC of the second and third band produce quasimomentum-matching conditions that lead to multi-refringence phenomena from a single incident beam without the introduction of defects into the lattice. Additionally, the coupling of a near-normal incident wave to a propagating almost perpendicular Bloch mode is shown to lead to strong right-angle redirection and collimation of the incident acoustic beam. Each effect is demonstrated both numerically and experimentally for scattering of ultrasound at a 10-period PnC slab in water environment. © 2022 Acoustical Society of America. https://doi.org/10.1121/10.0010158

(Received 8 December 2021; revised 18 March 2022; accepted 22 March 2022; published online 21 April 2022)

[Editor: Michael R Haberman] Pages: 2723–2731

I. INTRODUCTION

Phononic crystals are artificial structures with designed periodic arrangements¹ that can be characterized as "acoustic semiconductors" in select frequency ranges.² Within the low-frequency limit, the structures behave as effective media^{3–5} making them ideal for engineering physical properties for practical applications.^{6,7} At higher frequencies, abnormal and nonlinear dispersion of sound within a transmission band may give rise to peculiar effective media, such as hyperbolic dispersion of sound.^{8,9} Metamaterials have particularly drawn interest due to their ability to achieve index of refraction less than 1.0, including negative index of refraction.^{11,12} These unique properties can result in acoustic devices that demonstrate subwavelength resolution, ^{13–18} self-collimation, ^{9,10,19,20} cloaking, ^{21,22} and pulse decomposition.²³

Of interest here is the capability of phononic metamaterials to exhibit multi-refringence. In systems with two-dimensional (2D) or three-dimensional (3D) periodicity, multi-refringence becomes possible due to Laue diffraction at a set of periodically distributed scatterers. A plane wave incident at phononic crystal excites a number of Bloch waves, which satisfies the condition of conservation of tangential component of wave vector and appropriate symmetry

In the special case of normal incidence, the momentum-matching condition is irrelevant. Here, excitation of the Bloch mode with quasimomentum in the direction perpendicular to the direction of the incident wave may occur due to asymmetric shape of the scatterers,³³ Poisson-like effect,³⁴ or

¹Department of Physics, University of North Texas, Denton, Texas 76203, USA

²Echonovus Inc., Denton, Texas 76205, USA

³Department of Mechanical Engineering, University of North Texas, Denton, Texas 76207, USA

condition. These excited waves may propagate in different directions, thus generating multi-refringent beams. If the excited Bloch mode has anomalous dispersion, it may suffer very strong diffraction and propagate in the direction that is opposite to the "natural" direction-a phenomenon similar to negative refraction.²⁴ The introduction of defects²⁵ or cavities²⁶ into phononic crystals has been broadly used to engineer wave separation.²⁷ However, whereas the introduction of defects opens propagating modes or local states primarily in stop bands, shifts in the equifrequency contours (EFCs) away from the center of the Brillouin zone in defect-free crystals can result in multiple propagating phase matching conditions being allowed in transmission bands. ^{28,29} Anisotropy in the shape of EFCs, leading to angular dependence of index of refraction in an air-solid phononic crystal, was studied in Ref. 28. Also, positive, negative, and zero index of refraction were observed to occur in addition to passive birefringent beamsplitting due to quasimomentum matching conditions in the fourth transmission band. Similar conditions were utilized to realize splitting of sound waves passing through elastic phononic crystal prism³⁰ and sound through 2D water/steel PnC.³¹ It was shown that a topological Weyl phononic crystal exhibits positive or negative refraction depending on the crystallographic surface illuminated by incident wave.³²

a)Current address: University of North Texas, Center for Agile and Adaptive Additive Manufacturing, Denton, TX 76207, USA.

b)Current address: Institute of Fundamental and Frontier Sciences, University of Electronic Science and Technology of China, Chengdu 611731, China.

c)Electronic mail: arkady@unt.edu

symmetry of the EFCs centered at the points of high symmetry in Brillouin zone.²⁹ Even if the scattering system is uniform along the direction of propagation, e.g., a narrow slit of fluid clad between two metal plates, a resonant excitation in the perpendicular direction may occur because the uniform flatness of the boundaries of the slit is broken by acoustic vibrations.^{35,36}

Here, we explore the peculiar effects in reflection and transmission of sound through a phononic crystal slab associated with square-like EFCs. Multi-refringence at different angles of incidence occurs due to Umklapp scattering of an acoustic beam at the surface of a PnC. The term Umklapp scattering is borrowed from solid state physics where collision of two thermal phonons with quasimomenta k₁ and k₂ may create a phonon with quasimomentum exceeding the size of the Brillouin zone, $k_3 = k_1 + k_2 + G$. The Umklapp processes are allowed in periodic structures since Bloch vector is not true momentum but quasimomentum. Two waves with wave vectors \mathbf{k} and $\mathbf{k} + \mathbf{G}$ describe the same vibrational states, if G is one of the reciprocal lattice vectors. Due to this "uncertainty", the total momentum during scattering at a periodic potential is not necessarily conserved. Elastic scattering of electromagnetic waves (x rays) at ideal crystal leads to a set of maxima, so-called "reflections" in the diffraction pattern. The directions to the reflections \mathbf{k}' are related to the direction k of the incoming wave through Laue equation $\mathbf{k}' - \mathbf{k} = \mathbf{G}$, which describes Umklapp scattering of X-rays. Here, Umklapp scattering of sound waves must be explored through the overlap of the EFC of the ambient medium and that of the PnC. In contrast to the more well-known interpretations of scattering that come from analysis of the irreducible or first Brillouin zone, peculiar scattering conditions arise from overlaps outside the first Brillouin zone.

We use a PnC with fully symmetric scatterers arranged in a square lattice. This structure can give rise to EFCs that exhibit shifts away from the center of the Brillouin zone. These shifted EFCs can result in multiple phase matching conditions being allowed in the transmission band without necessarily coupling differing wave polarizations, crystal orientation dependent modes, or defects. An offset of EFCs contours belonging to the second and third transmission bands provide coupling of nearly normal incident rays to perpendicularly propagating modes in the crystal. These perpendicular modes are shown to suffer negative total internal refraction where energy propagates in the bulk of the crystal, but towards the direction of the emitting source. Multiband excitation has usually been realized in solid topological phononics by exciting both longitudinal and transversal modes³⁷ or using multifrequency source.³⁸ Multi-refringence and negative total internal refraction is examined both numerically and experimentally in a solid- fluid phononic crystal where the ambient only supports propagation of longitudinal pressure waves.

II. METHODS AND EXPERIMENTAL SETUP

The phononic crystal (PnC) is comprised of $1000 (100 \times 10) 1.59 \, \text{mm}$ diameter, $100 \, \text{mm}$ tall stainless-steel rods in a square lattice arrangement of lattice constant $a = 1.98 \, \text{mm}$

[Fig. 1(A)]. Rods are stabilized between two CNC machined Teflon plates that serve as the base and top, spaced 70 mm apart.

The EFCs and band structure were numerically calculated by the plane wave expansion method using intervals of 0.01 between -0.5 and 0.5 for k_x and k_y , measured in units of $2\pi/a$. Numerical simulations of acoustic transmission were performed using COMSOL Multiphysics software (COMSOL, Inc., Burlington, MA). A 100 × 10 array of stainless-steel rods were centered in a 220 mm × 100 mm water ambient area with absorption boundary conditions such that plane waves do not experience reflection at the boundaries. Water properties were taken from the COMSOL library with speed of sound c = 1480 m/s at 295 K ambient temperature, and density of 998 kg/m³. The Young's modulus, speed of sound, and density of tool steel were set to 200 GPa, 5800 m/s (longitudinal), 3100 m/s (transversal), and 7850 kg/m³, respectively. The ultrasound source was represented by a 25.4 mm (1") wide pressure line source placed 20 mm right of crystal center with incident angle varying from 10°-40° in 10° increments. Numerical results for the scattered acoustic intensity were calculated at 570 kHz.

Figure 1(B) is a schematic illustration of the experimental setup. All measurements were performed in a 0.55 m \times 0.55 m \times 0.55 m acrylic tank filled to a depth of \approx 0.38 m with DI water for full immersion of all samples and equipment. Ultrasound was emitted using a 1" Olympus V301 0.5 MHz immersion transducer (Olympus IMS, Waltham, MA), and detection using a 0.5 mm Müller-Platte (Oberursel, Germany) needle hydrophone. For controlling the incident angle, the V301 transducer was attached to a Thorlabs (Newton, NJ) CR1-Z6 angular translation stage where the incident angle is controlled to $\pm 0.5^{\circ}$. Pulses were generated with a JSR DPR300 pulser/receiver (Imaginant, Pittsford, NY) and acquired by a Tektronix MDO 3024 b (Newmark Systems, Beaverton, OR). The hydrophone was attached to a 2D Newmark LC-200-11 linear stage (Rancho Santa Margarita, CA) controlled by a Newmark NSG-G2-X2 stage controller to raster scan the transmission area for data acquisition.

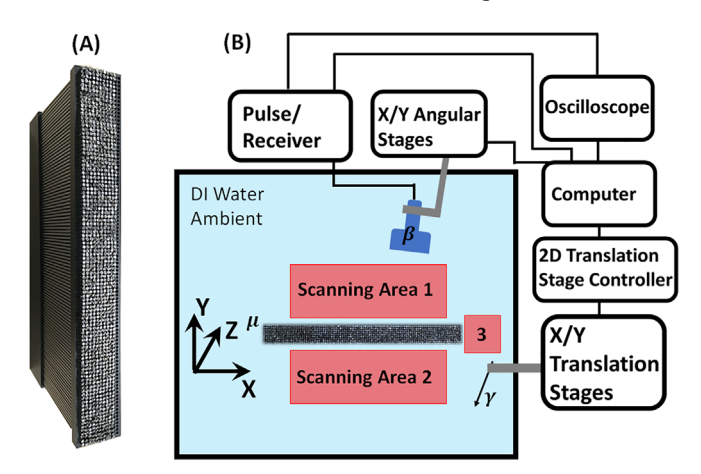


FIG. 1. (Color online) Fabricated phononic crystal and experimental setup. (A) Image of the phononic crystal of 100×10 scatterers. (B) Schematic diagram of the experimental setup. The acoustic beam is incident on the largest side of the crystal (μ) from a plane wave transducer (β) . A needle hydrophone (γ) is used for signal detection at pre-set grid points.

The experimental procedure starts with rotating the source to a predetermined incident angle. Negative spike pulses at 450 V amplitude and 100 Hz repetition rate were then generated with the DPR300 where signals were acquired with the needle hydrophone through a raster scan of areas on the incident (Area 1), transmitted (Area 2), and bulk plane (Area 3) of the phononic crystal [Fig. 1(B)]. Area 1 and Area 2 were zones of $120 \,\mathrm{mm} \times 40 \,\mathrm{m}$, where Area 1 starts 8 mm from the crystal boundary, and Area 2, starts 3 mm from the transmission boundary. The zone for Area 3 is $40 \,\mathrm{mm} \times 40 \,\mathrm{mm}$ and begins $3 \,\mathrm{mm}$ from the crystal edge. All raster data were acquired in 2 mm increments with a MATLAB (Mathworks, Natick, MA) script used to ensure 15 s of stationary data acquisition at each raster point. For each point, 512 samples are averaged and a fast Fourier transform performed using a Hanning window for frequency data. The resulting sound intensity maps were generated using MATLAB with a color map of sound intensity in the dB scale. For Area 1, the temporal data were used to distinguish between the incident and reflected pulse envelopes.

III. RESULTS

A. Band structure and equifrequency contours

Funneled collimation of sound by the same PnC was registered within a narrow range of frequencies in a metamaterial lens around 570 kHz. 17 Observations of multiple refracted beams from a single incident beam in Ref. 17

resulted in the necessity to study multi-refringence in the PnC, specifically at the collimation frequency of the metamaterial lens. The phononic crystal used in Ref. 17 thus served as the design guide for this work. From Fig. 2(A), the first transmission band of the PnC extends to 400 kHz from the origin as signified by the complete bandgap that occurs between 400 and 470 kHz.

For 2D PnC, the dispersion relation $\omega = \omega(k_x, k_y)$ can be represented as 3D plot for each transmission band. Cross-of these plots give the set of EFCs $\omega(k_x, k_y) = const$, which allow visualization of acoustic anisotropy and distribution of group velocities. Figures 2(B)–2(D) exhibit 3D plots of the dispersion in the first, second, and third band, respectively, with EFCs projected onto the $k_x - k_y$ plane. The linear dispersion in the first band extends to 250 kHz. Since the phononic crystal possesses a fourth-order rotational axis parallel to the rods, the linear dispersion is isotropic, i.e., the EFCs are represented by circles. For higher frequencies, the dispersion becomes nonlinear and the EFCs become anisotropic, keeping the rotational symmetry of order 4.

The effects of nonlinear dispersion can be seen in the contours of the second band in Fig. 2(C). They are centered in the Brillouin zone and maintain approximately square shapes with wide flat regions that are indicative of self-collimation. 9,19,20 Transition from the second to the third band is accompanied by a Van Hove singularity, i.e., by change of topology of equifrequency contours which in the third band is represented by open curves. Different topology is due to

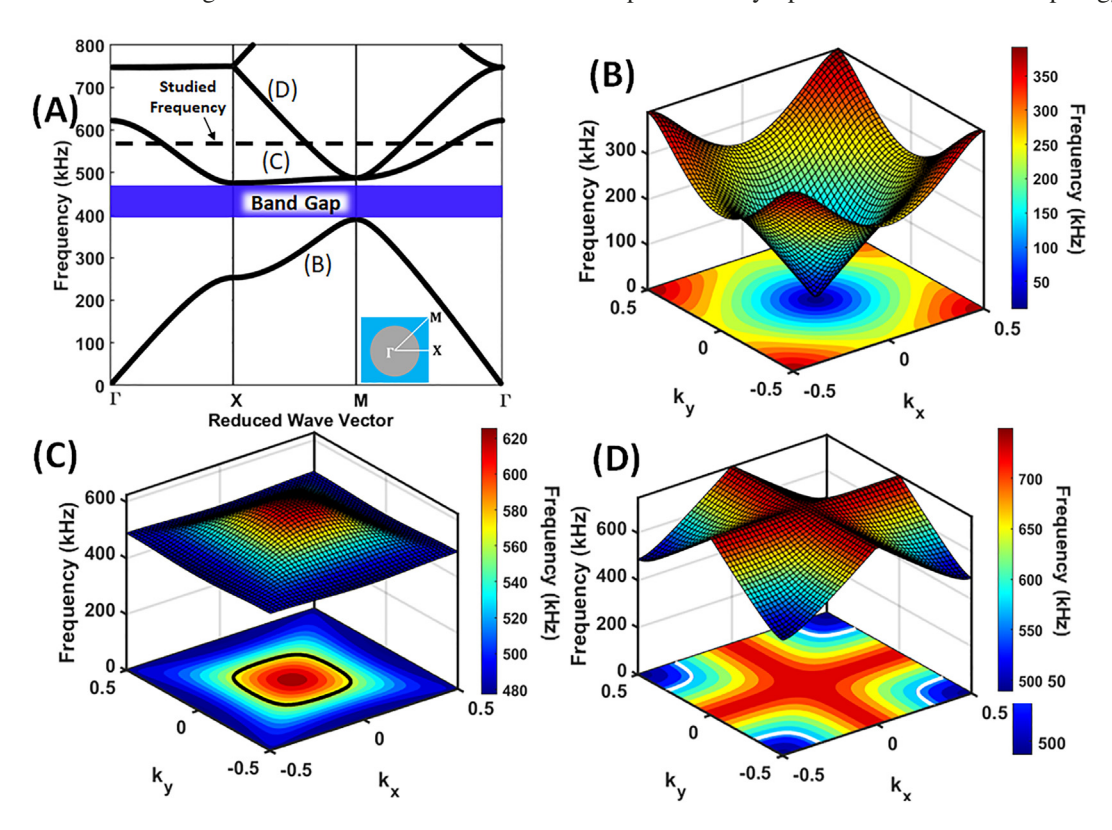


FIG. 2. (Color online) Calculated band structure and EFCs of the PnC. (A) Band structure of the crystal between 0 to 800 kHz along ΓX , XM, and $M\Gamma$ directions with Bloch vector measured in units of $2\pi/a$. The operating frequency of this study (570 kHz) is highlighted with a black dash line. (B)–(D) are the EFCs of the first, second, and third transmission bands in the first Brillouin zone. The lines corresponding to operating frequency, 570 kHz, is in bold black (C) and white (D).

JASA

the off-center shift by $(\pm 0.5, \pm 0.5)$ of each EFC. Similar shift results in birefringence observed in an air-solid PnC. ²⁸ Different topology of the equifrequency contours in the second and third bands leads to the inversion of the gradients (group velocities) with respect to the center of the Brillouin zone. This inversion and degeneracy at 570 kHz give rise to the effects discussed in Sec. III B.

B. Index of refraction

The approximately square EFC of the phononic crystal presents the opportunity to observe strong metamaterial effects. Wide flat regions on the EFCs are a source of singularities of the effective index of refraction. In homogenous media, the parallel nature of the group \mathbf{v}_g and phase \mathbf{v}_{ph} velocity contributes to an index of refraction defined in terms of the phase velocity $n=c_a/v_{ph}$, where c_a is the speed of sound in the medium surrounding the PnC (water in our case). However, where a material possesses acoustic anisotropy and nonlinear dispersion, the group velocity $\mathbf{v}_g = \nabla_{\mathbf{k}}\omega$ is more appropriately descriptive as it defines both the speed and direction of the propagation of energy carried by wave. Snell's law yields the group index of refraction n_g reported in Ref. 39;

$$n_g = -\frac{k_x}{k_0 \cdot \left(\frac{\partial k_y}{\partial k_x}\right)} \sqrt{1 + \left(\frac{\partial k_y}{\partial k_x}\right)^2}, \quad k_0 = \frac{\omega}{c_a}.$$
 (1)

Here, k_x and k_y are the tangential and normal to the PnC surface components of the vector **k** (see Fig. 1). Figure 3 provides the EFCs and associated group index of refraction calculated using Eq. (1). From Fig. 3(A), it is apparent that the group index for the second band remains negative for nearly all the wave vectors. It reaches very large negative values along the flat horizontal part of each EFC, where $|\partial k_y/\partial k_x| \ll 1$ except a narrow region near the origin where $k_x \to 0$.

For each mode with given k_x on the EFC, there are two modes with positive and negative *y*-projection of group velocity. In calculation of the group index, the mode with positive *y*-projection was used since it corresponds to the mode propagating towards the PnC (see Fig. 1). The directions of the group velocities in Fig. 3 are marked by blue (second band) and red (third band) arrows. Note the group velocities in the second band are directed outside-in and for the third band, they are directed inside-out, according to the evolution of the EFCs with frequency shown in Figs. 2(C) and 2(D).

Close inspection of n_g versus angle of incidence θ_i for the second and third bands shows the largest negative indices of refraction to occur and nearly normal incident angles [see Fig. 3(C)]. Negative refraction occurs for all except a small subset of incident angles. For small θ_i , large $|n_g|$ means that the angle of refraction is also small, i.e., the refracted rays propagate nearly normal to the incident surface, forming a set of collimated rays.

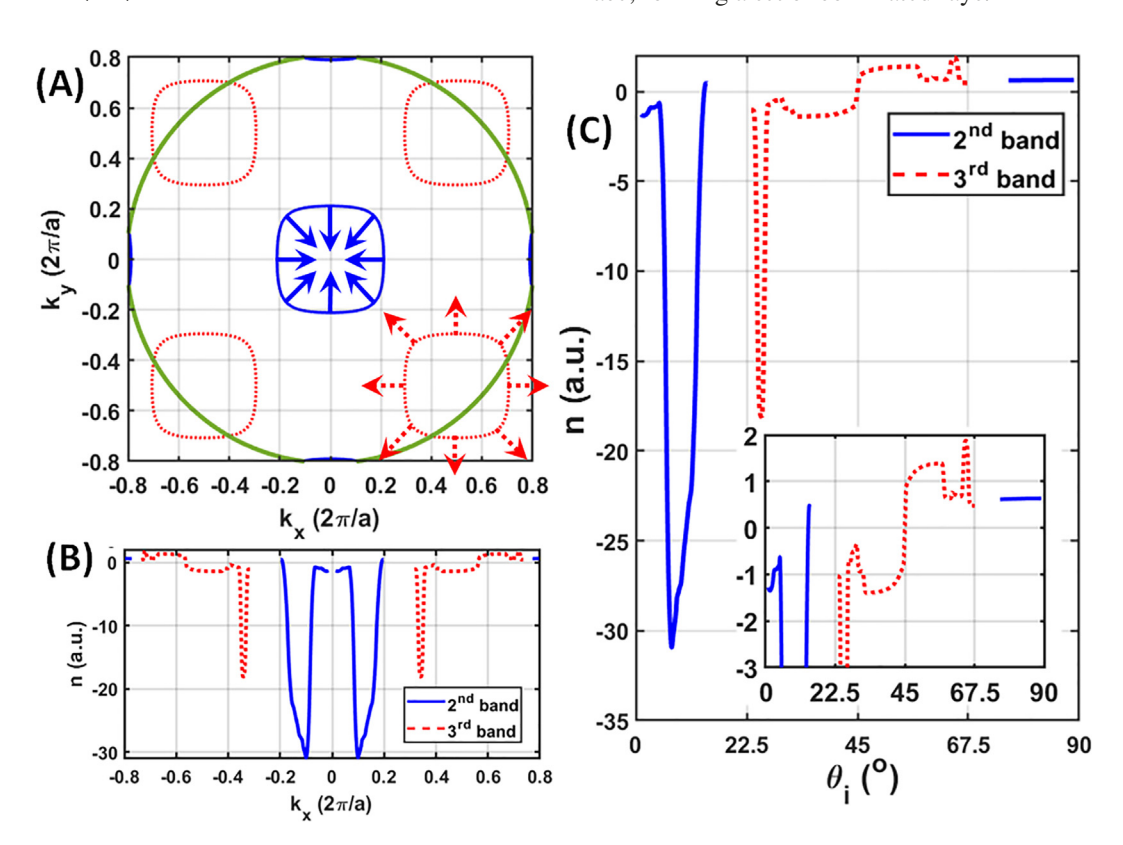


FIG. 3. (Color online) (A) EFCs in the second and third transmission bands corresponding to frequency 570 kHz. Arrows show the directions of group velocity. Green circle is the EFC for water. (B) Group index as calculated using Eq. (1). (C) Group index vs angle of incidence θ_i . Insert shows the blowup of the region where group index takes relatively small values.

C. Simultaneously positive and negative refraction and reflection

Equifrequency contours serve as the interpretive tool of the behavior of diffracted rays for a given angle of incidence, θ_i . Momentum matching at the interface of the phononic crystal and environment medium (water) requires that the tangential components of the incoming and refracted wave may differ by a reciprocal lattice vector,

sin theta_i
$$\frac{\omega}{c_a} = k_x(\omega) + \frac{2\pi m}{a}, \quad m = 0, \pm 1, \pm 2, \pm 3, \dots$$
 (2)

Analysis using EFCs is achieved in tandem with Eq. (2) in reciprocal lattice space. Water, the ambient material, possesses linear dispersion with an EFC represented by a green circle of radius ω/c_a in Fig. 3(A). At fixed angle of incidence θ_i and frequency ω , the roots of Eq. (2) give the set of allowed Bloch waves. By the same reasoning, it can also be seen that a propagating Bloch wave with fixed projection $k_x(\omega)$ excites a set of plane waves propagating in the ambient medium at angles $\theta_i(m)$ obtained from Eq. (2).

The effect of multi-refringence can be seen from the graphical solution of Eq. (2) demonstrated by Fig. 4. The incident beam with wave vector OA (black solid arrow) hits the surface of phononic crystal at angle θ_i . The EFC of water is represented by the relatively large green circle. The effect of multi-refraction appears because the incoming beam excites several Bloch waves in the third transmission band. In particular, the incident plane wave in Fig. 4 excites two refracted Bloch waves. They are obtained as intersections of vertical magenta lines with the red EFCs. Their wave vectors, *OB* and *OD*, satisfying Eq. (2) with m = 0 and m = -1are shown by red dash arrows. At higher frequencies, more Umklapp processes with $m = \pm 2, \pm 3, \dots$ become accessible. The group velocities of the refracted waves are shown by red solid arrows. For the refracted wave, the solutions of Eq. (2) with negative y-projection of group velocity are selected. The solutions with positive projections give rise to multi-reflection. Two Bloch waves suffer inverse refraction at the bottom surface of the sample. Leaving the crystal, the

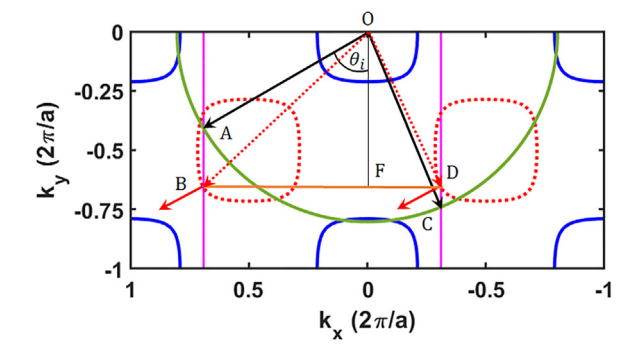


FIG. 4. (Color online) Geometrical interpretation of the solutions of quasimomentum-matching condition [Eq. (2)]. The wave vector of the incident wave \overrightarrow{OA} has equal y-projection with zero-order refracted wave represented by vector \overrightarrow{OB} and with first-order wave with wave vector \overrightarrow{OC} . Refracted waves are those with negative y-projection of the group velocity.

0th-order refracted mode (m=0) propagates in water parallel to the incident wave. However, the 1st-order mode (m=-1) leaves the crystal with wave vector \vec{OC} which propagates in a different direction.

While according to the directions of the group velocities at points *B* and *D* the incident wave exhibits positive refraction at the upper surface of the PnC, the direction of the outgoing wave suffering from Umklapp scattering corresponds to negative refraction at the bottom side of the sample.

The pattern of transmitted, reflected, and refracted rays changes with the angle of incidence θ_i . Figures 5(D)–5(F) show numerically simulated and Figs. 5(G)–5(I) show experimental results for the sound intensity field at different angles of incidence. The solutions of Eq. (2) are obtained through the geometrical construction of Fig. 4 and the outgoing rays are numerated from 1 to 4. The rays 1 (transmitted) and 2 (reflected) result from the 0th order scattering and the rays 3 (reflected) and 4 (transmitted) originate from the Umklapp process with m=-1.

Simultaneous negative and positive refraction and reflection can be observed in the phononic crystal when $k_{\rm r}(\omega)$ falls onto a horizontal surface of the PnC EFC. Figures 5(A)-5(B) show two momentum matching conditions satisfied for propagation through the phononic crystal from the 0th and 1st order diffraction modes. Subsequently, rays 2 and 3 illustrate standard reflection and backscattering. The latter can be considered as negative reflection as ray 3 is reflected back in the incident plane. Negative reflection in particular is a 1st order diffraction effect. The rays 1 and 4 are the transmitted waves, suffering, respectively, positive and negative refraction. The transmitted rays exhibit shifts in horizontal plane according to the directions of their group velocities. At $\theta_i = 20^\circ$, propagation through the crystal is forbidden due to lack of available propagation states [Fig. 5(C)]. However, here the fundamental and 1st order reflection modes still appear with negative reflection again being a 1st order effect [Figs. 5(F) and 5(I)]. The intensity of the transmitted rays 1 and 4 is very weak. It is different from zero only due to the finite thickness of the sample and presence of the Fourier components in the incoming beam corresponding to the angles different from $\theta_i = 20^{\circ}$. The scattering pattern observed in the experiment coincides well with the results obtained from Eq. (2). All the rays predicted by Eq. (2) were registered in the experiment and in the numerical modelling.

If the wave vector of the refracted wave obtained from Eq. (2) falls near a vertical boundary of an EFC, the group velocity, $\mathbf{v}_g = \nabla_{\mathbf{k}} \omega(k)$, is primarily in the plane of the phononic crystal [Fig. 6(A)]. The result is practically right-angle scattering of the incident ray leading to the apparent propagation of acoustic energy parallel to the interface of the PnC. This situation is realized at $\theta_i = 10^\circ$. In Fig. 6, the incident wave is split into two rays, which leaving the crystal, appear in the ambient medium as rays 1 and 2. The projection $k_x(\omega)$ falls near the edge of the EFC of the second band centered at $k_x = 0, k_y = -1$. As the group velocity of the second transmission band is directed outside-in, two

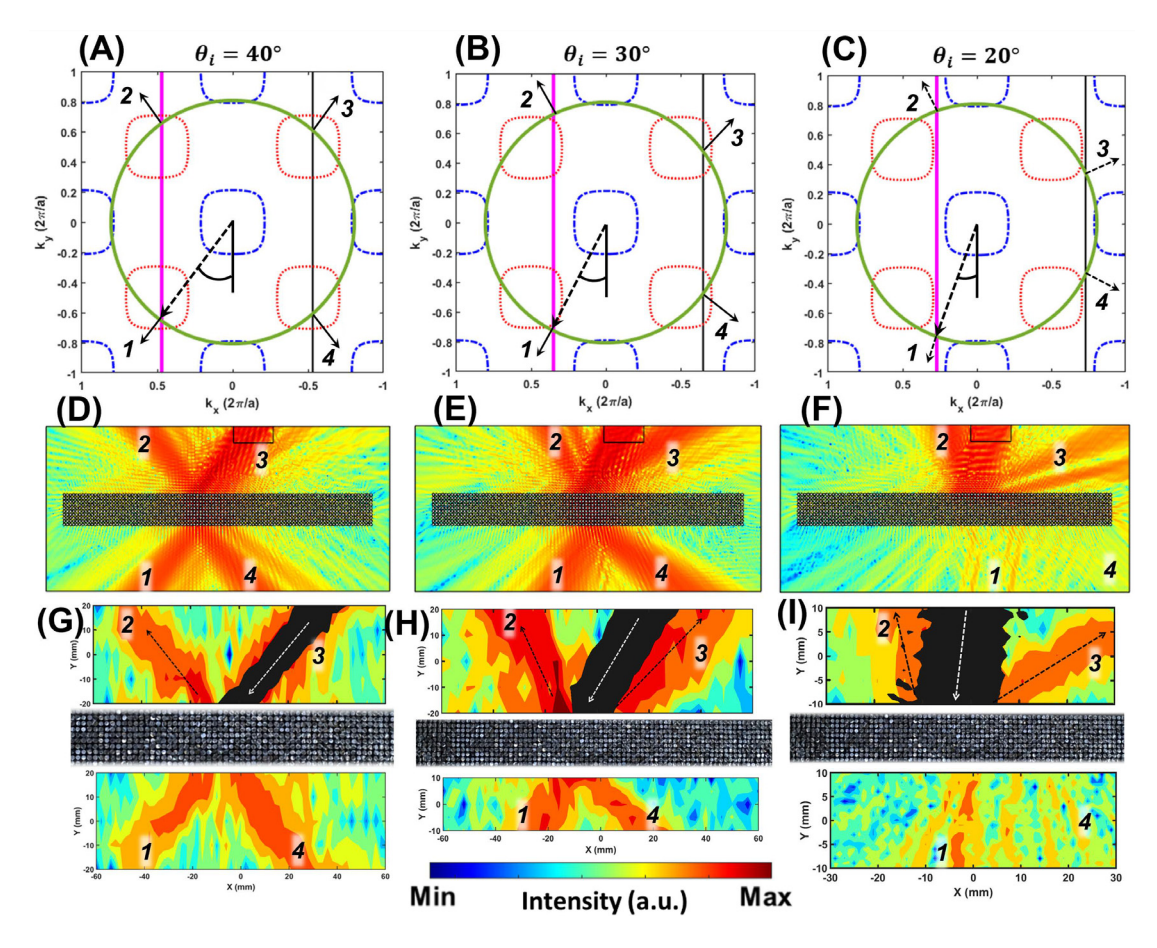


FIG. 5. (Color online) Equifrequency contours (A)-(C), numerically simulated (COMSOL) sound pressure fields (D)-(F) and measured sound intensity fields (G)-(I) of the phononic crystal at 40°, 30°, and 20°. Ultrasound is emitted from a 1" source for the numerical and experimental results. The direction of the incident wave in (G)–(I) is marked by white arrow.

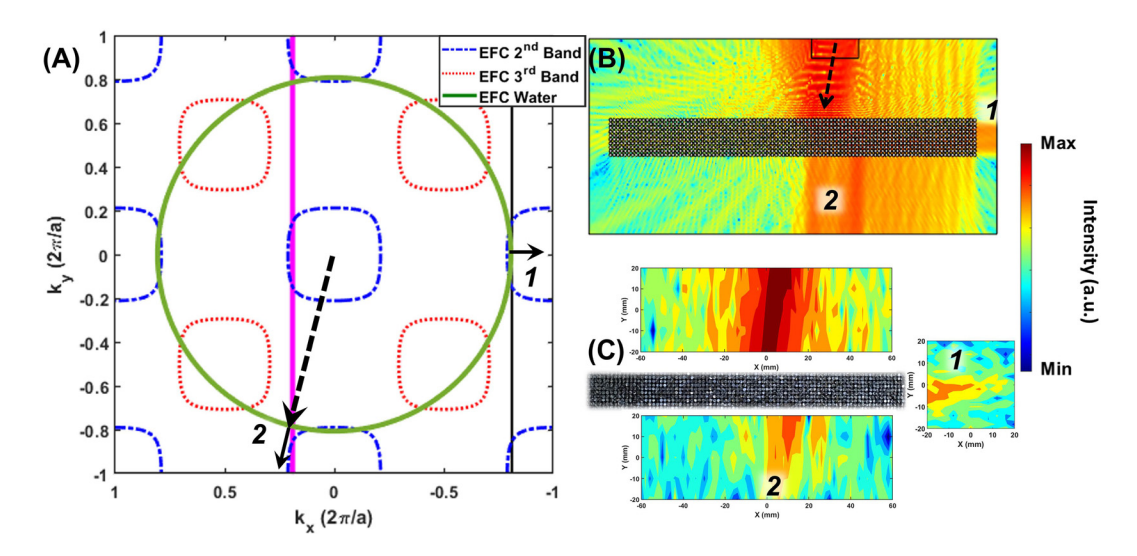


FIG. 6. (Color online) The behaviors of the phononic crystal with a 10° incident (respected to normal line) beam angle. (A) The equifrequency contours of the second (blue dashed-dotted contours) and third transmission (red dot contours) bands with 6 × 6 Brillouin zones at 570 kHz. The green solid circle refers to the EFC of water ambient at 570 kHz. The incident beam is represented by the dashed black arrow. The group velocity vectors in water ambient and in the phononic crystal are shown by small black and red arrows, respectively. The vertical solid magenta and dark green lines indicate the momentummatched condition Eq. (2) with m = 0, 1. (B) Numerically simulated sound intensity field. (C) Experimental mapped sound intensity fields of incidence area and transmission area with size 120 mm by 40 mm.

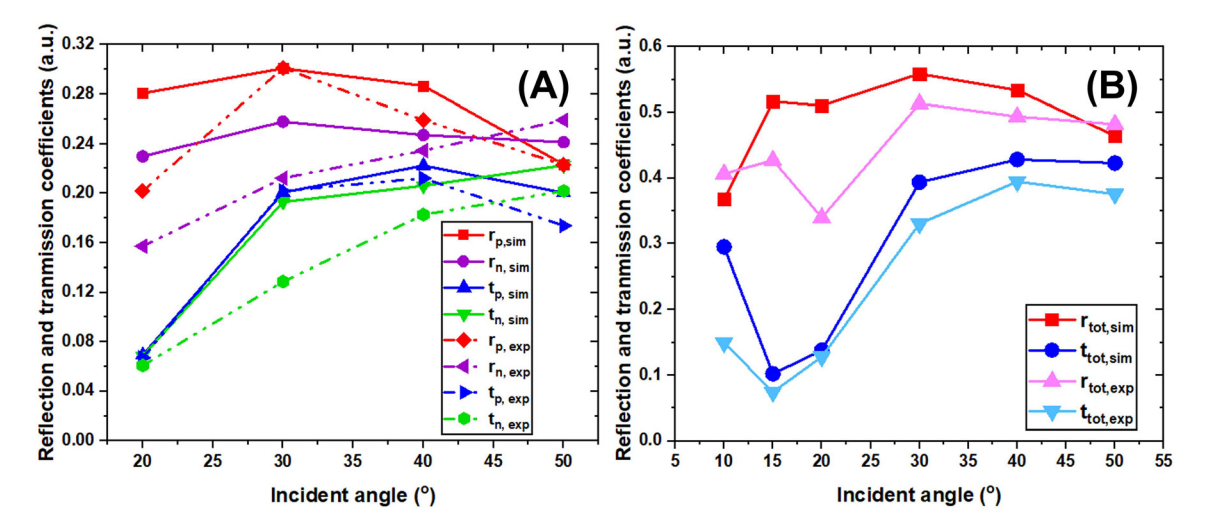


FIG. 7. (Color online) Transmission and reflection coefficients from both simulation and experimental sound fields for some descrete values of incident angles, including those shown in Fig. 5. (A) The reflection and transmission coefficients for positively (p) and negatively (n) reflected and transmitted rays. The values are taken from average absolute pressure amplitude of the centers of the incident, reflected, and transmitted rays. (B) The total transmission and reflection coefficients which account for all the transmitted and reflected rays. Scattering results in coefficients do not sum to one, and thus, the coefficients only give relative information, not absolute.

refracted Bloch waves propagate against the "natural" direction, i.e., towards the incident source, exhibiting strong negative refraction.

Ray 1 originates from an Umklapp scattering of the incident wave. Due to low curvature of the EFC, this ray is well collimated. This results in relatively intensive beam, which leaves the sample in the direction practically perpendicular to the incident ray [see Figs. 6(B) and 6(C)]. Similar strong redirection of sound incident at a periodic chain of metal scatterers was reported in Ref. 24. In geometrical optics, propagation of the refracted ray parallel to the interface is a signature of total internal reflection. It is observed when the incident wave comes from optically more dense medium. This condition is evidently satisfied since the size of EFC for water is larger than that for phononic crystal. However, the ray 1 cannot be considered as a result of negative total internal reflection since for the angles of incidence $\theta_i > 10^{\circ}$, this ray does not become an evanescent mode. It propagates in the bulk parallel to the interface of the sample. Note that the right-angle bend of sound was previously observed using the methods of transformation acoustics, which require a metamaterial medium with continuously changing index of refraction. 40 Another approach to bend a sound beam requires application of a pentamode material.⁴¹

The fundamental mode (m=0) couples into ray 2, which leaves the sample parallel to the incident ray. While the direction of this ray corresponds to standard refraction, it can be seen in Figs. 6(B) and 6(C) that its point of exit from the sample is anomalously shifted. This occurs because this ray suffers negative refraction at the interface. The direction of the group velocity of the refracted wave is shown by red arrow in Fig. 6(A). According to the direction of the group velocity, the ray 2 is shifted towards the incident source. The reason for the anomalous shift and negative refraction is anomalous dispersion of the Bloch wave in the second

band. Note that the group index in Fig. 3 reaches its most negative values near $\theta_i = 10^\circ$.

The strong multi-refringence effects present the ability to manipulate energy strength along with direction. As the phononic crystal causes significant scattering, here, we limit the definition of the coefficients to the ratio of the amplitude of sound pressure at the centers of incident, reflected, and transmitted rays. Figure 7 illustrates the reflection and transmission coefficients for both simulated and experimental results for all angles examined. Partial coefficients accounting for positive and negative reflection and refraction are plotted in Fig. 7(A). While the amount of sound energy scattered to each channel is different, all four plots exhibit similar angular dependence. More broadly, a total reflection (transmission) coefficient is determined by accounting for all reflected (transmitted) channels simultaneously and the results shown in Fig. 7(B). Since these values do not account for the pressure distributed over the whole width of each beam, the reflection and transmission coefficients will not necessarily sum to 1. There are also dissipative and scattering losses over the PnC sample. The values plotted in Fig. 7, while they do not correspond to the standard definitions, still grant insight into the relative strength of reflected and transmitted rays. From Fig. 7, it is apparent that energy redirection and modulation is achievable through control of the incident angle. Whereas variation as 1.6 times can be realized for reflection, transmission varies as much as 5.3 times for $15^{\circ} < \theta_i < 40^{\circ}$. Though redirection and energy manipulation are able to be realized, there is insufficient control to manipulate each independently.

IV. CONCLUSIONS

In summary, simultaneous negative and positive refraction and reflection were experimentally observed and numerically modelled for 2D phononic crystal with square

JASA

lattice. Experimental and numerical results for the distribution of scattering intensity are in a good agreement with analytical momentum-matching condition [Eq. (2)]. The symmetry of square lattice and square-like shape of the equifrequency contours results in a critical angle about which the overlapping interception of the second and third bands with the excitation frequency causes inversion of positive/negative ray directions between the two bands. For these higher bands, analysis of the extended Brillouin zones finds angles that exhibit not only multi-refringence caused by Umklapp scattering but the coupling of near-normal incident waves to perpendicularly propagating Bloch waves, resulting in strongly anomalous scattering and redirection of the incident wave. The coupling of near-normal incident waves to waves that propagate perpendicular to the plane of incidence in phononic crystals has been extensively investigated through surface acoustic waves, 32,42 Lamb waves, 43 and Rayleigh waves. 44 However, these waves either require the ability for elastic wave propagation, occur in thin films, or only occur near the surface due to the evanescent nature of surface modes. Here, it is demonstrated that the appropriate phononic crystal can couple incident pressure waves to an allowed Bloch mode propagating in the bulk.

ACKNOWLEDGMENTS

This work is supported by the National Science Foundation under EFRI Grant No. 1741677.

- ¹M. S. Kushwaha, P. Halevi, L. Dobrzynski, and B. Djafari-Rouhani, "Acoustic band structure of periodic elastic composites," Phys. Rev. Lett. **71**, 2022–2025 (1993).
- ²J. P. Dowling, "Sonic band structure in fluids with periodic density variations," J. Acoust. Soc. Am. **91**, 2539–2543 (1992).
- ³J. Berryman, "Long-wavelength propagation in composite elastic media I. Spherical inclusions," J. Acoust. Soc. Am. 68, 1809–1819 (1980).
- ⁴A. Krokhin, J. Arriaga, and L. Gumen, "Speed of sound in periodic elastic composites," Phys. Rev. Lett. **91**, 264302 (2003).
- ⁵A. N. Norris, A. L. Shuvalov, and A. A. Kutsenko, "Analytical formulation of three-dimensional dynamic homogenization for periodic elastic composites," Proc. R. Soc. A **468**, 1629–1651 (2012).
- ⁶N. Zen, T. A. Puurtinen, T. J. Isotalo, S. Chaudhuri, and I. J. Maasilta, "Engineering thermal conductance using a two-dimensional phononic crystal," Nat. Commun. **5**, 3435 (2014).
- ⁷Y. Pennec, J. O. Vasseur, B. Djafari-Rouhani, L. Dobrzyński, and P. A. Deymier, "Two-dimensional phononic crystals: Examples and applications," Surf. Sci. Rep. **65**, 229–291 (2010).
- ⁸M.-H. Lu, L. Feng, and Y.-F. Chen, "Phononic crystals and acoustic metamaterials," Mater. Today 12, 34–42 (2009).
- ⁹V. M. García-Chocano, J. Christensen, and J. Sánchez-Dehesa, "Negative refraction and energy funneling by hyperbolic materials: An experimental demonstration in acoustics," Phys. Rev. Lett. 112, 144301 (2014).
- ¹⁰Z. He, F. Cai, Y. Ding, and Z. Liu, "Subwavelength imaging of acoustic waves by a canalization mechanism in a two-dimensional phononic crystal," Appl. Phys. Lett. **93**, 233503 (2008).
- ¹¹X. Zhang, "Negative refraction of acoustic waves in two-dimensional phononic crystals," Appl. Phys. Lett. 85, 341–343 (2004).
- ¹²J. Li, Z. Liu, and C. Qiu, "Negative refraction imaging of acoustic waves by a two-dimensional three-component phononic crystal," Phys. Rev. B 73, 054302 (2006).
- ¹³A. Sukhovich, L. Jing, and J. Page, "Negative refraction and focusing of ultrasound in two-dimensional phononic crystals," Phys. Rev. B 77, 014301 (2008).

- ¹⁴S. Peng, Z. He, H. Jia, A. Zhang, C. Qiu, M. Ke, and Z. Liu, "Acoustic far-field focusing effect for two-dimensional graded negative refractiveindex sonic crystals," Appl. Phys. Lett. 96, 263502 (2010).
- ¹⁵N. Kaina, F. Lemoult, M. Fink, and G. Lerosey, "Negative refractive index and acoustic superlens from multiple scattering in single negative metamaterials," Nature 525, 77–81 (2015).
- ¹⁶J. J. Park, C. M. Park, K. J. B. Lee, and S. H. Lee, "Acoustic superlens using membrane-based metamaterials," Appl. Phys. Lett. 106, 051901 (2015).
- ¹⁷E. L. Walker, Yu. Jin, D. Reyes, and A. Neogi, "Sub-wavelength lateral detection of tissue-approximating masses using an ultrasonic metamaterial lens," Nat. Commun. 11, 5967 (2020).
- ¹⁸T. Yang, Y. Jin, T.-Y. Choi, N. Dahotre, and A. Neogi, "Mechanically tunable ultrasonic metamaterial lens with a subwavelength resolution at long working distances for bioimaging," Smart Mater. Struct. 30, 015022 (2021).
- ¹⁹J. Christensen, A. I. Fernandez-Dominguez, F. de Leon-Perez, L. Martin-Moreno, and F. J. Garcia-Vidal, "Collimation of sound assisted by acoustic surface waves," Nat. Phys. 3, 851–852 (2007).
- ²⁰O. A. Kaya, A. Cicek, and B. Ulug, "Self-collimated slow sound in sonic crystals," J. Phys. D 45, 365101 (2012).
- ²¹X. Zhu, B. Liang, W. Kan, X. Zou, and J. Cheng, "Acoustic cloaking by a superlens with single-negative materials," Phys. Rev. Lett. 106, 014301 (2011).
- ²²A. N. Norris, "Acoustic cloaking theory," Proc. R. Soc. A **464**, 2411–2434 (2008).
- ²³Y. Jin, Y. Zubov, T. Yang, T.-Y. Choi, A. Krokhin, and A. Neogi, "Spatial decomposition of a broadband pulse caused by strong frequency dispersion of sound in acoustic metamaterial superlattice," Mater. 14, 125 (2020).
- ²⁴A. Bozhko, J. Sánchez-Dehesa, F. Cervera, and A. Krokhin, "Redirection and splitting of sound waves by a periodic chain of thin perforated cylindrical shells," Phys. Rev. Appl. 7, 064034 (2017).
- ²⁵X. K. Han and Z. Zhang, "Acoustic beam controlling in water by the design of phononic crystal," Extreme Mech. Lett. 34, 100602 (2020).
- ²⁶X. Li and Z. Liu, "Coupling of cavity modes and guiding modes in twodimensional phononic crystals," Solid State Commun. 133, 397–402 (2005).
- ²⁷Y. Pennec, B. Djafari-Rouhani, J. O. Vasseur, H. Larabi, A. Khelif, A. Choujaa, S. Benchabane, and V. Laude, "Acoustic channel drop tunneling in a phononic crystal," Appl. Phys. Lett. 87, 261912 (2005).
- ²⁸J. E. R. Bucay, J. O. Vasseur, P. A. Deymier, A. C. Hladky-Hennion, Y. Pennec, K. Muralidharan, B. Djafari-Rouhani, and B. Dubus, "Positive, negative, zero refraction, and beam splitting in a solid/air phononic crystal: Theoretical and experimental study," Phys. Rev. B 79, 214305 (2009).
- ²⁹X. Bai, C. Qiu, H. He, S. Peng, M. Ke, and Z. Liu, "Extraordinary lateral beaming of sound from a square-lattice phononic crystal," Phys. Lett. A 381, 886–889 (2017).
- ³⁰H. Lee, J. H. Oh, and Y. Y. Kim, "Multiple beam splitting in elastic phononic crystal plates," Ultrasonics 56, 178–182 (2015).
- ³¹R. P. Moiseyenko, S. Herbison, N. F. Declercq, and V. Laude, "Phononic crystal diffraction gratings," J. Appl. Phys. 111, 034907 (2012).
- ³²H. He, C. Qiu, L. Ye, X. Cai, X. Fan, M. Ke, F. Zhang, and Z. Liu, "Topological negative refraction of surface acoustic waves in a Weyl phononic crystal," Nature 560, 61–64 (2018).
- ³³X. Su and D. Banerjee, "Asymmetric lateral sound beaming in a Willis medium," Phys. Rev. Res. 3, 033080 (2021).
- ³⁴A. S. Titovich and A. N. Norris, "Acoustic Poisson-like effect in periodic structures," J. Acoust. Soc. Am. 139, 3353–3356 (2016).
- ³⁵V. M. García-Chocano, Nagaraj, T. López-Rios, L. Gumen, J. Sánchez-Dehesa, and A. Krokhin, "Resonant coupling of Rayleigh waves through a narrow fluid channel causing extraordinary low acoustic transmission," J. Acoust. Soc. Am. 132(4), 2807–2815 (2012).
- ³⁶A. Bozhko, V. Garcìa-Chocano, J. Sánchez-Dehesa, and A. Krokhin, "Redirection of sound in straight fluid channel with elastic boundaries," Phys. Rev. B 91, 094303 (2015).
- ³⁷S.-Y. Huo, J. J. Chen, H.-B. Huang, and G.-L. Huang, "Simultaneous multi-band valley-protected topological edge states of shear vertical wave in two-dimensional phononic crystals with veins," Sci. Rep. 7, 10335 (2017).
- ³⁸A. Ganesan, C. Do, and A. Seshia, "Excitation of coupled phononic frequency combs via two-mode parametric three-wave mixing," Phys. Rev. B 97, 014302 (2018).
- ³⁹J. Christensen and F. Javier Garcia de Abajo, "Anisotropic metamaterials for full control of acoustic waves," Phys. Rev. Lett. 108, 124301 (2012).

JASA

https://doi.org/10.1121/10.0010158

- ⁴⁰W. Lu, H. Jia, Y. Bi, Y. Yang, and J. Yang, "Design and demonstration of an acoustic right-angle bend," J. Acoust. Soc. Am. 142, 84–89 (2017).
 ⁴¹Z. Sun, H. Jia, Y. Chen, Z. Wang, and J. Yang, "Design of an underwater
- ⁴¹Z. Sun, H. Jia, Y. Chen, Z. Wang, and J. Yang, "Design of an underwater acoustic bend by pentamode metafluid," J. Acoust. Soc. Am. **143**, 1029–1034 (2018).
- ⁴²B. Ash, S. Worsfold, P. Vukasic, and G. R. Nash, "A highly attenuating and frequency tailorable annular hole phononic crystal for surface acoustic waves," Nat. Commun. 8, 174 (2017).
- ⁴³J. Zhao, R. Marchal, B. Bonello, and O. Boyko, "Efficient focalization of antisymmetric Lamb waves in gradient-index phononic crystal plates," Appl. Phys. Lett. 101, 261905 (2012).
- 44M. Oudich, B. Djafari-Rouhani, B. Bonello, Y. Pennec, S. Hemaidia, F. Sarry, and D. Beyssen, "Rayleigh waves in phononic crystal made of multilayered pillars: Confined modes, Fano resonances, and acoustically induced transparency," Phys. Rev. Appl. 9, 034013 (2018).